Optical Review
https://doi.org/10.1007/s10043-019-00561-z

REGULAR PAPER

# The image reconstruction for fluorescence molecular tomography via a non-uniform mesh

**Bin Wang[1] · Pu Jiao[1] · Huangjian Yi[1] · Xin Cao[1] · Fengjun Zhao[1] · Yuqing Hou[1] · Xiaowei He[1]**

Received: 24 April 2019 / Accepted: 31 October 2019


**Abstract**
As an optical molecular imaging modality, fluorescence molecular tomography (FMT) can monitor the activities of organisms in vivo at the molecular and cellular levels. However, the recovered image quality is affected by mesh voxel when the finite element method is utilized to recover the fluorescence probe. The target localization is likely to deviate from the actual target under the coarse mesh, but using the fine mesh will increase the number of unknowns, which makes the computational burden heavier and further aggravate the ill-posedness. To solve the problem, a reconstruction strategy using a non-uniform mesh for FMT is developed in this paper. The numerical experiment and physical experiment validated that the strategy is capable and effective for FMT.

**Keywords** Optical molecular imaging · Fluorescence molecular tomography · Finite element method · Non-uniform mesh

## 1 Introduction

Fluorescence molecular tomography (FMT), as an important alternative to molecular imaging, can achieve the three-dimensional visualization of fluorophore in tissues [1, 2]. By employing the fluorescent measurements and the appropriate model of propagation of near-infrared light in biological tissues, FMT can localize and quantify the fluorescence probe [3]. The imaging technique has been successfully applied to drug development and cancer diagnosis [4, 5].

The inverse problem in FMT has severe ill-posedness attributed to the high scattering photons propagated in biological tissues. The inverse problem is under-determined problem because of a large number of unknowns as well as a limited number of measurements [6]. To conquer this problem, considerable researches are proposed in recent years. For instance, Lian et al. [7] eliminate many unknown experimental factors with the help of a nonlinear normalized Born ratio (nBorn) method, which provides better localization and quantitative performance.

✉ Huangjian Yi
yhj2014@nwu.edu.cn

✉ Xiaowei He
hexw@nwu.edu.cn

[1] School of Information Sciences and Technology, Northwest University, Xi'an 710069, Shaanxi, China

Furthermore, the accuracy of the recovered image is affected by the size of the discrete mesh. M. Guven et al. [8, 9] proposed an error analysis framework for the relationship between discretization and reconstruction accuracy for FDOT (fluorescence diffuse optical tomographic). With this framework, two adaptive meshing algorithms based on error bound and the number of nodes are proposed. Numerical simulation results show that the accuracy, resolution and detectability of the reconstructed image are improved with noise-free. Further, considering the influence of the noise, L Zhou et al. [10] proposed an adaptive meshing algorithm based on the upper bound estimation of deviation and variance error in MSE. Simulation results show that this method is effective in the reconstruction process with noise. However, those methods above require a large number of optimization and iteration parameters, which increases the amount of reconstruction computation. Some researchers have also proposed mesh generation methods based on feasible regions and their subdivisions. For example, D. Wang et al. [11] presented an adaptive mesh method which divides the selected elements in the coarse mesh into eight equal sub-hexahedrons, which improves the amount of computation and the quality of reconstruction. However, this method only employed the subdivision mesh and did not fully consider the global information before and after mesh subdivision. Schultz et al. [12] developed and proposed a hybrid imaging method for FMT and X-ray computed tomography (XCT), and further proposed the

Published online: 16 November 2019

idea of using feasible region subdivision to improve the reconstruction quality. Yi et al. [13] extract a permissible region from the initial result with coarse mesh to guide the reconstruction using a fine discretization mesh, and it can obtain an improved distribution of fluorophore. However, it needs to create two different sizes of mesh, namely coarse and fine. How to identify a coarse and fine is a new problem.

In the current study, we present a non-uniform mesh for FMT on the purpose of optimizing the reconstruction precision. First, a rough result can be rapidly obtained on the coarse mesh, subdivide the area where the energy value of nodes is more than 20% of the maximum value as the permissible region. Then, the subdivision region is combined with the external coarse mesh to form a non-uniform mesh, on which the global reconstruction is carried out. To test the performance of the proposed method, the numerical simulation experiments and physical experiments are implemented, and the reconstruction results proved that the developed method can provide satisfying results in FMT.

The rest of the paper is organized as follows. Section 2 displays the forward problem and the developed approach; experiment setup and results are exhibited in Sect. 3; discussion and conclusion are presented in Sect. 4.

## 2 Methods

### 2.1 Forward problem

The propagation of near-infrared photons in biological tissues is characterized by high scattering and low absorption [14]. Then the radiative transfer equation (RTE) [19] is utilized to depict the propagation. However, it exists immense difficulties in the process of solving the equation. Hence, the photon diffusion equation (PDE), as an approximation of RTE, is commonly used to model the photon propagation. For steady-state FMT with point excitation sources, the following coupled diffuse equations can be utilized to depict the forward problem [15]:

$$\begin{cases} -\nabla \cdot (D_x(r)\nabla \Phi_x(r)) + \mu_{ax}(r)\,\Phi_x(r) = \Theta\delta(r - r_s) \\ -\nabla \cdot (D_m(r)\nabla \Phi_m(r)) + \mu_{am}(r)\,\Phi_m(r) = \Phi_x(r)\eta\,\mu_{af}(r) \end{cases} \quad (r \in \Omega) \tag{1}$$

where $\Omega$ denotes the three-dimensional space occupied by an imaging object.$r$ is the position vector and $r_s$ is the excitation source position. $D_x, D_m$ denote diffusion coefficients of excited light and fluorescence, separately.$\mu_{ax}, \mu_{am}$ are absorption coefficients of excitation light and fluorescence, respectively.$\Phi_x, \Phi_m$ denotes photon density of excitation light and fluorescence, respectively. $\eta\mu_{af}$ indicates the fluorescence probe distribution to be reconstructed. $\Theta$ denotes the amplitude of the point excitation source.

To solve the above equation, combined with Robin boundary and finite element method (FEM), Eq. (1) can be written as the following matrix equation:

$$\begin{aligned} K_x\,\Phi_x &= S_x, \\ K_m\,\Phi_m &= FX, \end{aligned} \tag{2}$$

where $K_x, K_m$ denote system matrix, respectively. $s_x$ is the distribution of excitation light source. By removing the non-measured values at both sides of the equation, the following linear relationships can be established:

$$WX = \Phi, \tag{3}$$

where $X$ is fluorescence yield, $W$ is system matrix and $\Phi$ represents the fluorescence photon density on the surface. Equation (3) can be transformed into an optimization problem utilizing regularization, as follows:

$$\min_x \frac{1}{2}\|WX - \Phi\|_2^2 + \tau\|X\|_1, \tag{4}$$

where $\tau$ is the regularization parameter and $\tau > 0$. Finally, incomplete variable-truncated conjugate gradient (IVTCG) algorithm [16] is used to recover the fluorescence target.

### 2.2 Non-uniform mesh

Using FEM to solve FMT, the reconstruction capability is always restricted by mesh thickness. Considering the computational cost, coarse mesh is always adopted for fast FMT, although the recovered localization is close to the real target, the gap between the reconstructed target and the real position is too large to meet the actual requirement. However, if mesh voxel is small, the unknowns will greatly increase, and the ill-condition of the inverse problem will be aggravated, so it is more difficult to solve the problem. To achieve a promising result, the paper seeks to provide a novel method with the help of non-uniform mesh. First, a coarse mesh is used to approximate the imaging object, and the initial reconstruction result is obtained, owing to the coarse mesh, the location error is larger, but this preliminary result can provide a permissible region for the next reconstruction. It is generally considered that the unit with a large fluorescence yield is an increased probability of a recovered target. Therefore, the node with high fluorescence yield is selected as the possible region of the target, that is, the permissible region is constructed, and further subdivision is carried out in this domain. Finally, the subdivision region is combined with the outer coarse mesh to form a non-uniform mesh, and then the final FMT reconstruction is conducted on the whole region. Figure 1 shows the schematic diagram of three kinds of mesh with different sizes and Fig. 1a–c is

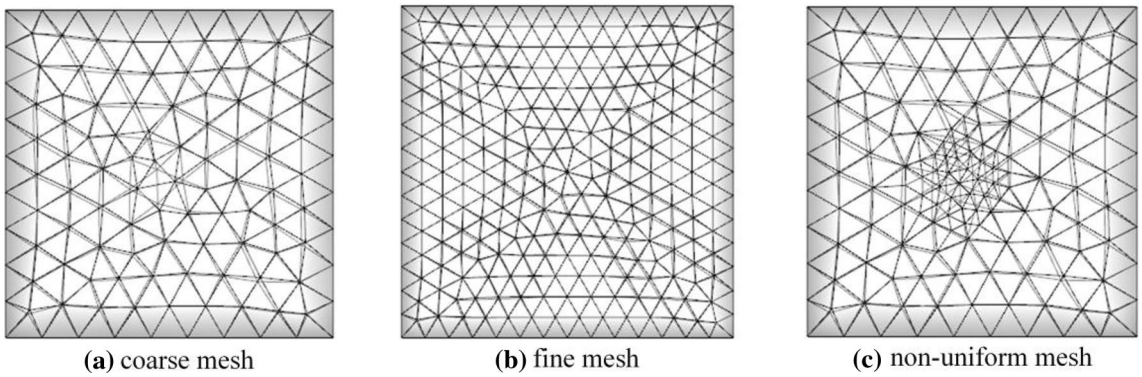


**Fig. 1** The schematic diagram of three kinds of mesh with different sizes

a schematic diagram of coarse mesh, fine mesh, and non-uniform mesh, respectively.

## 3 Experiment

Cylindrical simulation and physical phantom experiments are conducted to verify the feasibility of the proposed method. In this paper, three reconstructed images can be acquired by coarse mesh, non-uniform mesh, and fine mesh, separately. Then, according to location error (LE), we can form an evaluation for assessing the reconstruction quality. Where LE indicates the Euclidean distance between the recovered target position and the real target position, and the smaller the value is, the better the image quality. The calculation formula of LE is as follows:

$$LE = \sqrt{(x - x_0)^2 + (y - y_0)^2 + (z - z_0)^2} \tag{5}$$

where $(x, y, z)$ denotes the coordinates of the real fluorescent target and $(x_0, y_0, z_0)$ is the recovered light source.

### 3.1 Cylindrical simulation experiment

In the simulation experiment, the cylinder with a radius of 10 mm and a high 30 mm is regarded as the phantom, a smaller cylinder, a radius of 0.5 mm and a high 1.5 mm, is used as a fluorescent target and placed in the lung. The three-dimensional schematic is shown in Fig. 1, in which the red cylinder represents a fluorescent target. Moreover, the main organs of the cylindrical phantom include the heart, bone, lungs, muscle, and liver. The optical parameters of the main tissues and organs in the mouse model are shown in Table 1[17]. The fluorescence target coordinate is (0 mm,6 mm, 15 mm) in the cylindrical simulation experiment, and 18 excitation points are utilized to capture fluorescence measurements.

**Table 1** The optical parameters of major tissues and organs ($mm^{-1}$)

| Tissues and organs | $\mu_{ax}$ | $\mu'_{sx}$ | $\mu_{am}$ | $\mu'_{sm}$ |
|---|---|---|---|---|
| Heart | 0.0083 | 1.01 | 0.0104 | 0.99 |
| Lung | 0.0133 | 1.97 | 0.0203 | 1.95 |
| Liver | 0.0329 | 0.70 | 0.0176 | 0.65 |
| Muscle | 0.0052 | 1.08 | 0.0068 | 1.03 |

A three-dimensional diagram of a non-homogeneous cylinder is exhibited in Fig. 2a. Figure 2b is the three-dimensional diagram of inverse mesh.

In the process of coarse mesh reconstruction, the non-homogeneous cylinder model is discretized into 10,291 tetrahedral elements and 1884 nodes. Based on coarse mesh reconstruction, those nodes and tetrahedral elements which are more than a certain percentage threshold of the maximum fluorescence yield are selected as permissible regions for subdivision mesh. To illustrate the selection of feasible region threshold, we tested the percentage threshold of several different maximum fluorescence yields and their effects on the LE. The experimental results show that 10–70% of the maximum fluorescence yield has no significant effect on the LE, as shown in Table 2. But when the threshold reaches 80% or more of the maximum fluorescence yield, there are too few nodes and tetrahedral elements for subdivision, thus affecting the quality of reconstruction. To take into account the LE and the amount of data subdivided into grids, 20% of the maximum fluorescence yield is selected as the threshold.

Figure 3 shows the results of reconstruction applying three kinds of meshes sizes. Figure 3a–c is the recovered images of coarse mesh, fine mesh, and non-uniform mesh, respectively. Table 3 is the quantitative analysis of reconstruction quality. From Fig. 3 and Table 3, the LE of reconstruction result of coarse is 1.53 mm, which seriously deviates from the real fluorescence target. However, the image quality of fine mesh has not been improved obviously, although the LE is reduced to 1.19 mm, the increase of

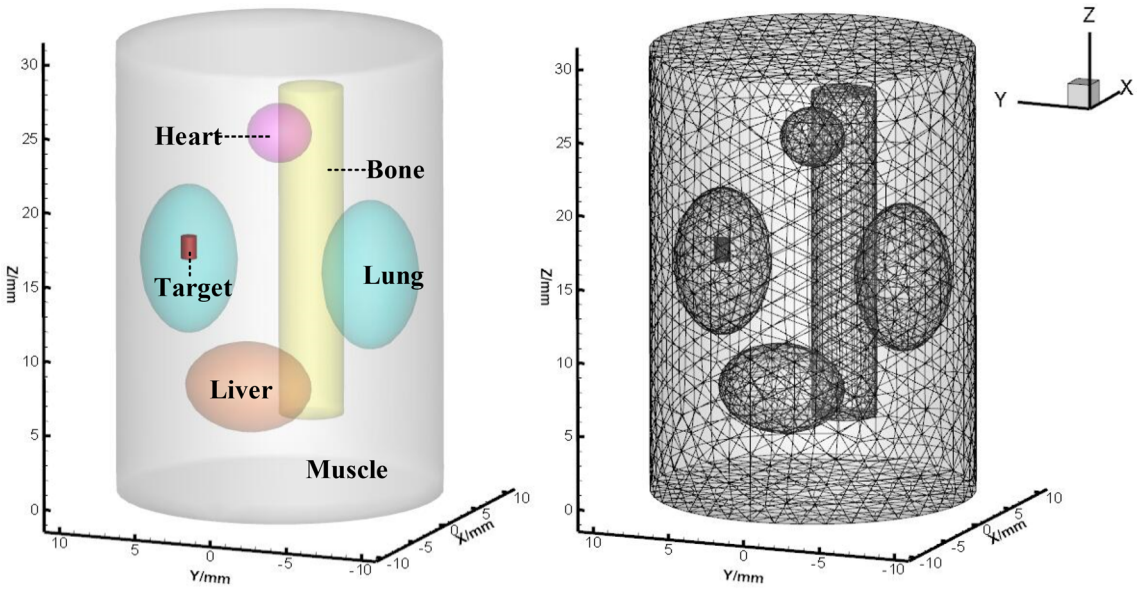


(a) Three-dimensional diagram of a non-homogeneous cylinder

(b) mesh subdivision of Cylinder phantom

**Fig.2** Three-dimensional diagram of a non-homogeneous cylinder

**Table 2** The quantitative analysis of reconstruction quality and subdivision unit under different threshold

| Threshold | LE/mm | Number of units to subdivide | Volume to subdivide |
|---|---|---|---|
| 5% | 0.50 | 5105 | 2120.39 |
| 10% | 0.52 | 337 | 104.84 |
| 20% | 0.52 | 337 | 104.84 |
| 40% | 0.52 | 282 | 88.57 |
| 50% | 0.52 | 282 | 88.57 |
| 60% | 0.52 | 139 | 38.76 |
| 70% | 0.52 | 139 | 38.76 |
| 80% | 1.53 | 47 | 17.96 |

unknowns make the computational burden heavier and take a lot of time to calculate iteratively, so the distribution of fluorescence probe cannot be obtained quickly and effectively. Table 4 is the quantitative analysis of reconstruction time. From Table 4, in the forward problem, the time of using the non-uniform grid to calculate the system matrix is about the same as that of the coarse grid, but much lower than that of the fine grid. In the inverse problem, the reconstruction time of non-uniform mesh is less than that of coarse mesh and fine mesh. Compared with the above result, the result of the proposed method is ideal, the reconstructed localization is extremely close to the real target and the LE is only 0.51 mm, the reconstruction accuracy is greatly improved with less reconstruction time and storage space.

We evaluated the performance of the proposed method by taking into consideration the influence of noise. The simulations were conducted on a non-homogeneous cylinder by considering the measured data at different levels (5%, 10%, 15%, 20%, and 25%) of the additive Gaussian noise. Figure 4 shows the corresponding results at each noise level. Table 5 shows that in the aspect of the LE of reconstruction when using the non-uniform grid, with the increase of the intensity of Gaussian noise, the LE of reconstruction also increases. However, the LE of 5% and 10% noise levels is still lower than that of coarse grid and fine grid, and the 15% noise level is close to the LE of coarse grid. In terms of calculation time, the calculation time of the system matrix and the fine mesh division time of the permissible region increase with the increase of noise intensity, but it is much lower than the calculation time of fine grid.

### 3.2 Physical phantom experiment

To further validate the feasibility of the proposed method, physical experiments were carried out. The square of side length 20 mm, the material of polyformaldehyde, is employed as a physical phantom. A cylindrical hole with a diameter of 2 mm and a high 2 mm was drilled into the cube as the fluorescence target, Cy5.5 fluorescent dye was injected into it. The real target is set in the (16.0 mm, 8.0 mm, and 9.5 mm). The optical parameters of physical phantom refer to [18]. Four excitation points were set around the phantom and four groups of fluorescence measurements

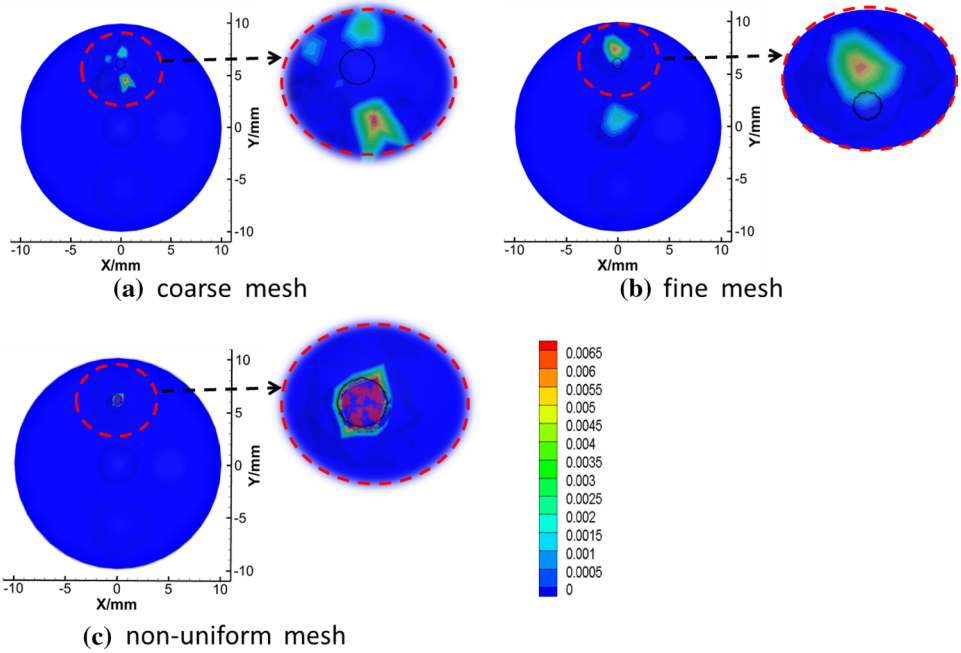


**Fig.3** The results of reconstruction applying three kinds of meshes sizes

**Table 3** The quantitative analysis of reconstruction quality under different meshes sizes

| Grid | Nodes/tetrahedron | Real source center/mm | Reconstructed source center/mm | LE/mm |
|---|---|---|---|---|
| Coarse mesh | 1884/10,291 | (0, 6, 15) | (− 0.03, 7.47, 14.69) | 1.53 |
| Fine mesh | 10,936/61,964 | (0, 6, 15) | (0.19, 7.07, 15.48) | 1.19 |
| Non-uniform mesh | 5545/30,630 | (0, 6, 15) | (− 0.03, 5.99, 15.51) | 0.51 |

**Table 4** The quantitative analysis of reconstruction time under different mesh sizes

| Grid | Nodes/tetrahedron | System matrix time/s | Reconstructed time/s |
|---|---|---|---|
| Coarse mesh | 1884/10,291 | 30.77 | 1.81 |
| Fine mesh | 10,936/61,964 | 107.33 | 2.13 |
| Non-uniform mesh | 5545/30,630 | 31.54 | 0.49 |

were collected by charge-coupled device (CCD) camera. Figure 5a, b displays a schematic diagram of physical phantom and excitation point setting, respectively.

Figure 6 is the section diagram of reconstruction results at $z = 9.5$ mm under the three kinds of mesh. Figure 6a–c is the reconstruction images by a coarse mesh, a fine mesh, and a non-uniform mesh. We can conclude by analyzing the recovered images that the recovered quality with coarse mesh is very unsatisfactory, the reconstructed area with fluorescence yield has two places and is far from the real fluorescence marker. Moreover, the LE of fine mesh is not obviously reduced and cannot provide accurate localization. However, the method proposed in this paper can obtain high image quality, and the LE is greatly reduced.

## 4 Conclusion and discussion

Due to the ill-posed problem of the inverse problem in the FMT, it is necessary to gather a large scale of fluorescent measurements for inversion, which leads to the reconstruction slow down and be unable to effectively locate targets in real time. For the sake of raising the accuracy of FMT reconstruction, this paper represents an innovative method based on the non-uniform mesh, the mesh near the target will be subdivided, while the other domain is divided under the coarse level. In our experiments, all results approved of the proposed method, in the case of moderate calculation, can locate the fluorescent target

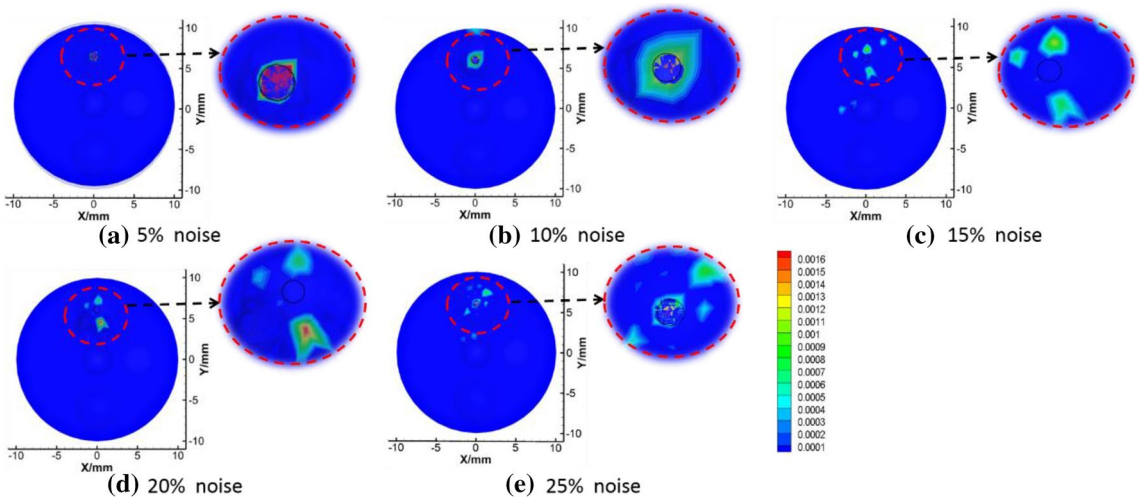


**Fig.4** The results of reconstruction utilizing five level of noise case using non-uniform mesh

**Table 5** The quantitative analysis of reconstruction quality and time under different levels noise case using non-uniform mesh

| Noise level | Real source center/mm | Reconstructed source center/mm | LE/mm | System matrix time/s | Remesh time/s | Reconstructed time/s |
|---|---|---|---|---|---|---|
| 5% | (0, 6, 15) | (− 0.04, 6.09, 15.47) | 0.52 | 27.43 | 26.72 | 0.54 |
| 10% | (0, 6, 15) | (− 0.19, 5.88, 15.85) | 0.88 | 28.35 | 29.31 | 0.77 |
| 15% | (0, 6, 15) | (− 0.30, 7.47, 14.69) | 1.53 | 36.56 | 41.89 | 1.51 |
| 20% | (0, 6, 15) | (0.40, 4.67, 16.47) | 2.02 | 35.38 | 34.44 | 1.27 |
| 25% | (0, 6, 15) | (0.15, 7.24, 16.64) | 2.06 | 38.69 | 38.68 | 1.50 |

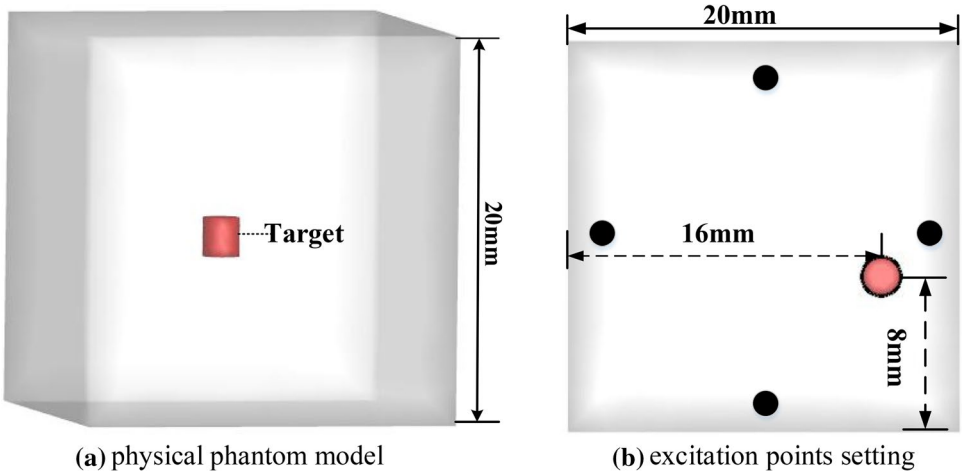


**Fig.5** The schematic diagram of physical phantom and excitation point setting

more accurately and improve the reconstruction precision than existing algorithms.

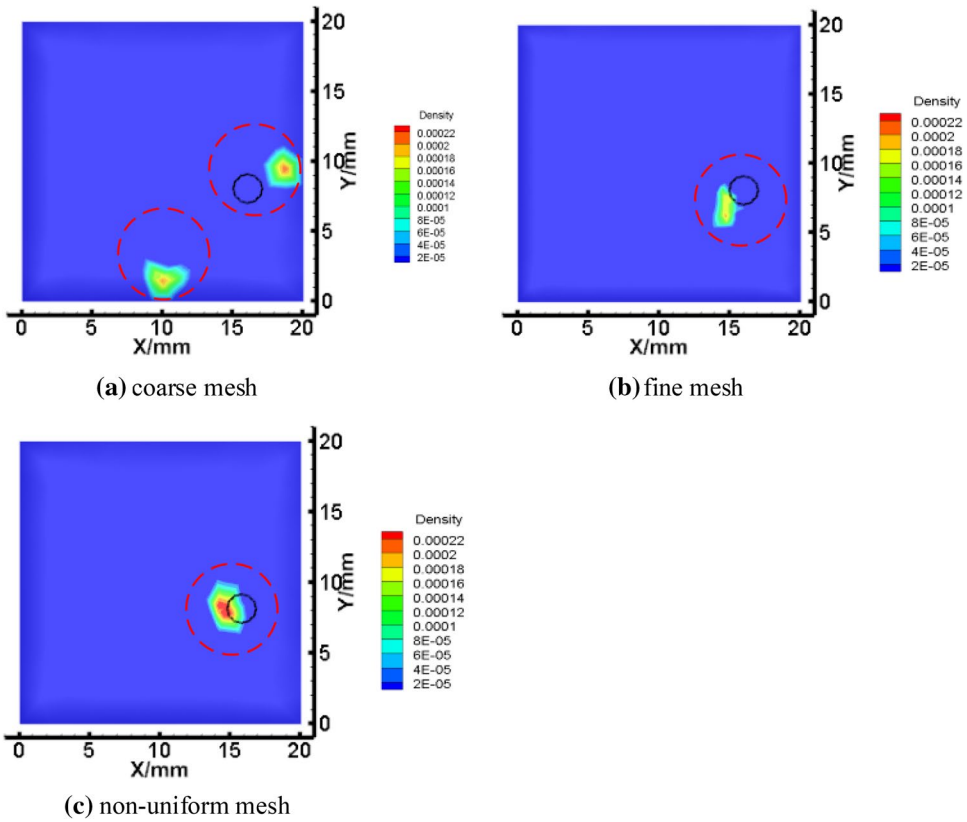


**(a)** coarse mesh **(b)** fine mesh

**(c)** non-uniform mesh

**Fig. 6** The section diagram of reconstruction results at $z = 9.5$ mm under the three kinds of mesh

## Compliance with ethical standards

**Conflict of interest** We declare that we have no financial and personal relationships with other people or organizations that can inappropriately influence our work, there is no professional or other personal interest of any nature or kind in any product, service and/or company that could be construed as influencing the position presented in, or the review of, the manuscript entitled "The image reconstruction for fluorescence molecular tomography via a non-uniform mesh".

## References


1. Ntziachristos, V., Tung, C.-H., Bremer, C., Weissleder, R.: Fluorescence molecular tomography resolves protease activity in vivo. Nat Med. **8**(7), 757–761 (2002)
2. Bai, J., Xu, Z.: Molecular Imaging: Fundamentals and Applications, pp. 185–216. Springer, Berlin (2013)
3. Xu, C., Xin, W., Zhang, B., Fei, L., Luo, J., Jing, B.: Accelerated image reconstruction in fluorescence molecular tomography using dimension reduction. Biomed Opt Express. **4**(1), 1–14 (2013)
4. Vasilis, N., Schellenberger, E.A., Jorge, R., Doreen, Y., Edward, G., Alexei, B., Lee, J., Ralph, W.: Visualization of antitumor treatment by means of fluorescence molecular tomography with an annexin V-Cy5.5 conjugate. Proc Natl Acad Sci USA **101**(33), 12294–12299 (2004)
5. Dimarzio, C.A., Niedre, M.: Pre-clinical optical molecular imaging in the lung: technological challenges and future prospects. J Thorac Dis **4**(6), 556–557 (2012)
6. Chen, D., Liang, J., Li, Y., Qiu, G.: A sparsity-constrained preconditioned Kaczmarz reconstruction method for fluorescence molecular tomography. BioMed Res Int **2016**, Article ID: 4504161 (2016)
7. Lian, L., Deng, Y., Xie, W., Xu, G., Yang, X., Zhang, Z., Luo, Q.: Enhancement of the localization and quantitative performance of fluorescence molecular tomography by using linear nBorn method. Opt Express **25**(3), 2063–2079 (2017)
8. Guven, M., Reilly-Raska, L., Zhou, L., Yazıcı, B.: Discretization error analysis and adaptive meshing algorithms for fluorescence diffuse optical tomography: Part I. IEEE Trans Med Imaging. **29**(2), 217–229 (2010)
9. Guven, M., Reilly-Raska, L., Zhou, L., Yazici, B.: Discretization error analysis and adaptive meshing algorithms for fluorescence diffuse optical tomography: Part II. IEEE Trans Med Imaging **29**(2), 230–245 (2010)
10. Zhou, L., Yazici, B.: Discretization error analysis and adaptive meshing algorithms for fluorescence diffuse optical tomography in the presence of measurement noise. IEEE Trans Image Process **20**(4), 1094–1111 (2010)
11. Wang, D., Song, X.L., Bai, J.: Adaptive-mesh-based algorithm for fluorescence molecular tomography using an analytical solution. Opt Express. **15**(15), 9722–9730 (2007)
12. Schulz, R.B., Angelique, A., Athanasios, S., Marcus, F., Eric, S., Marta, Z., Vasilis, N.: Hybrid system for simultaneous fluorescence and x-ray computed tomography. IEEE Trans Med Imaging **29**(2), 465–473 (2009)
13. Yi, H., Zhang, X., Peng, J., Zhao, F., Wang, X., Hou, Y., Chen, D., He, X.: Reconstruction for limited-projection fluorescence molecular tomography based on a double-mesh strategy. Biomed Res Int **2016**, Article ID: 5682851 (2016)
14. Yi, H., Jiao, P., Li, X., Peng, J., He, X.: Three-way decision based reconstruction frame for fluorescence molecular tomography. J. Opt. Soc. Am. **35**(11), 1814–1822 (2018)

15. Han, D., Tian, J., Zhu, S.P., Feng, J.C., Qin, C.G., Zhang, B., Yang, X.: A fast reconstruction algorithm for fluorescence molecular tomography with sparsity regularization. Opt. Express. **18**(8), 8630–8646 (2010)
16. Xiaowei, H., Jimin, L., Xiaorui, W., Jingjing, Y., Xiaochao, Q., Xiaodong, W., Yanbin, H., Duofang, C., Fang, L., Jie, T.: Sparse reconstruction for quantitative bioluminescence tomography based on the incomplete variables truncated conjugate gradient method. Opt Express. **18**(24), 24825–24841 (2010)
17. Hou, Y., Hua, X., Xin, C., Zhang, H., Xuan, Q., He, X.: Single-view enhanced cerenkov luminescence tomography based on sparse bayesian learning. Acta Optica Sinica. **37**(12), 298–308 (2017)
18. Guo, H., Hou, Y., He, X., Yu, J., Cheng, J., Xin, P.: Adaptive hp finite element method for fluorescence molecular tomography with simplified spherical harmonics approximation. J. Innov. Opt. Health Sci. **7**(2), Article ID 1350057 (2014)
19. Klose, A.D., Ntziachristos, V., Hielscher, A.H.: The inverse source problem based on the radiative transfer equation in optical molecular imaging. J. Comput. Phys. **202**(1), 323–345 (2005)